RSC Advances

PAPER

View Article Online
View Journal | View Issue



Cite this: *RSC Adv.*, 2015, **5**, 84754

# $ACdCO_3F$ (A = K and Rb): new noncentrosymmetric materials with remarkably strong second-harmonic generation (SHG) responses enhanced *via* π-interaction†

Guohong Zou,[a] Gnu Nam,[b] Hyung Gu Kim,[a] Hongil Jo,[a] Tae-Soo You*[b] and Kang Min Ok*[a]

Received 25th August 2015
Accepted 30th September 2015

DOI: 10.1039/c5ra17209h

www.rsc.org/advances

Two new noncentrosymmetric (NCS) materials, namely, $ACdCO_3F$ (A = K and Rb) containing both a $d^{10}$ cation ($Cd^{2+}$) and a π-conjugated parallel carbonate anion ($CO_3^{2-}$), were synthesized through conventional solid state reactions. $ACdCO_3F$ exhibits a 3-dimensional structure that is composed of the stacked layers of $[Cd(CO_3)]_\infty$. Each $[Cd(CO_3)]_\infty$ layer is connected by infinite Cd–F–Cd chains and the $[CO_3]$ triangles are oriented in the same direction with a coplanar alignment. $KCdCO_3F$ and $RbCdCO_3F$ reveal remarkably strong second-harmonic generation (SHG) responses of approximately 9.0 and 7.2 times that of potassium dihydrogen phosphate (KDP), respectively, and both materials are phase-matchable. $ACdCO_3F$ exhibit wide transparent regions ranging from far UV to mid IR. Theoretical calculations confirm that the large SHG efficiencies indeed originate from enhancement *via* interatomic interactions between the s and p states of $Cd^{2+}$ and the π-conjugated groups of the $[CO_3]^{2-}$ unit within the $[Cd(CO_3)]_\infty$ layers.

## Introduction

The increasing importance of ultraviolet (UV) and deep-UV nonlinear optical (NLO) materials,[1] as the key component of all-solid-state UV and deep-UV lasers, has prompted the continuous exploitation of new NLO crystals with high NLO coefficients and wide UV transparency. In general, a good UV or deep-UV NLO material should meet the following four criteria: (1) a relatively larger SHG coefficient ($d_{ij}$) than that of KDP; (2) a moderate birefringence (0.07–0.1) to achieve the phase matching condition in the UV region; (3) a wide UV transparency range and high damage threshold; and (4) good chemical stability and mechanical properties. Thus far, metal borates NLO materials,[2] such as β-$BaB_2O_4$,[2b] $LiB_3O_5$,[2c] $KBe_2BO_3F_2$,[2d] and $SrBe_2BO_7$,[2e] satisfying most of the above conditions have been the focus of intensive investigations. Over the last few decades, many efforts have been made to understand the relationship between the composition/structure and the NLO properties. According to the anionic group theory proposed by Chen,[3] the boron–oxygen anionic groups have the dominant contribution to the macroscopic optical responses of the UV and deep-UV NLO borates. Several well-known examples of NCS borates are found from $[B_3O_6]^{3-}$ in β-$BaB_2O_4$,[2b] $[B_3O_7]^{5-}$ in $LiB_3O_5$,[2c] $CsB_3O_5$,[2f] and $CsLiB_6O_{10}$,[2g,2h] $[BO_3]^{3-}$ in $KBe_2BO_3F_2$,[2d] $SrBe_2BO_7$,[2e] $K_2Al_2B_2O_7$,[2i] and $[BO_4]^{5-}$ in $Li_2B_4O_7$.[2j] In particular, the planar $[BO_3]^{3-}$ anionic group, with a moderate birefringence and a large microscopic second-order susceptibility $\beta$, is considered to be the best NLO basic structural unit for UV and deep-UV light generation.

Meanwhile, the $[CO_3]^{2-}$ anionic group that is isoelectronic with $[BO_3]^{3-}$ unit can also be used as a building block to design best performing UV NLO materials. In addition, most of carbonates possess good physical and chemical properties; thus, materials with $[CO_3]^{2-}$ groups have invoked specific interests. In fact, several new carbonate NLO materials drawing much attention have been synthesized recently. Leblanc's group reported a series of NCS $K_4Ln_2(CO_3)_3F_4$ (Ln = Nd, Sm, Eu and Gd).[4] Ye's group introduced alkali metal fluorides into carbonates and successfully synthesized a family of novel fluoride carbonates, $MNCO_3F$ (M = K, Rb, Cs; N = Ca, Sr, Ba)[5a] which are promising UV NLO materials with moderate SHG coefficients. Ye and co-workers also discovered a few more NCS mixed metal fluoride carbonates such as $Na_8Lu_2(CO_3)_6F_2$,[5b] $Na_3Lu(CO_3)_2F_2$,[5b] and $CsPbCO_3F$.[5c] Halasyamani's group recently synthesized $K_{2.70}Pb_{5.15}(CO_3)_5F_3$ [6a] and $RbPbCO_3F$[6b] along with a new deep-UV NLO material, $RbMgCO_3F$.[6c]

It has been known that the increased density of the planar π-conjugated groups and its alignment could improve the NLO

[a]*Department of Chemistry, Chung-Ang University, Seoul, 156-756, Republic of Korea*
[b]*Department of Chemistry, Chungbuk National University, Cheongju, Chungbuk, 361-763, Republic of Korea. E-mail: kmok@cau.ac.kr; tsyou@chungbuk.ac.kr; Fax: +82 2 825 4736; Tel: +82 2 820 5197*

† Electronic supplementary information (ESI) available: Atomic coordinates and isotropic displacement parameters, selected bond distances and angles, infrared spectra, PXRD patterns of thermal decomposition products, and COHP curves for $KCdCO_3F$ and $RbCdCO_3F$. See DOI: 10.1039/c5ra17209h

performance of extended solid state materials. Other well established noncentrosymmetric (NCS) chromophores that can enhance stronger SHG efficiencies in extended structures are found from the polar displacement of a $d^{10}$ cation center[7] and second-order Jahn–Teller (SOJT) distortive cations such as $d^0$ transition metal cations with octahedral coordination environment and lone pair cations.[1a,1b,8] A couple of successfully designed interesting NLO materials include $Cd_4BiO(BO_3)_3$ [7a] and $CsPbCO_3F$.[5c] Guided by this idea, we introduced $Cd^{2+}$ cation into carbonates for two reasons: (1) because $Cd^{2+}$ is a divalent cation with the similar ionic radius to that of $Ca^{2+}$, the coplanarity and alignment of $[CO_3]^{2-}$ triangles can be easily maintained in the structure of $KCaCO_3F$,[5a] which can result in a moderate birefringence for the phase matching condition in the UV region; (2) the polyhedra of $d^{10}$ cation, $Cd^{2+}$, can interact with the π-conjugated $[CO_3]^{2-}$ units and may reveal synergistic polar displacement effect. Our investigations of the A–Cd–$CO_3$–F (A = alkali metals) system resulted in two new alkali metal cadmium fluoride carbonates, *i.e.*, $ACdCO_3F$ (A = K and Rb). Although the coordination environment of $Cd^{2+}$ cation is highly symmetrical in the $CdO_6F_2$ polyhedron, it shows higher electronic deformation ability than that of $KCaCO_3F$. We will demonstrate that the strong π-interaction between $Cd^{2+}$ and $[CO_3]^{2-}$ groups within the $[Cd(CO_3)]$ layers is responsible for the remarkable SHG response for the first time.

# Experimental section

## Synthesis

Polycrystalline samples of $ACdCO_3F$ (A = K and Rb) were synthesized through standard solid-state reactions. Stoichiometric amounts of KF (Alfa Aesar, 99%) or RbF (Alfa Aesar, 99%) and $CdCO_3$ (Alfa Aesar, 99%) were thoroughly mixed with agate mortars and pestles and pressed into pellets. The pellets were heated at 320 °C for 80 h, and cooled down to room temperature rapidly at a rate of 10 °C $min^{-1}$ with several intermediate grinding steps in between each heating. Synthesized NCS $KCdCO_3F$ and $RbCdCO_3F$ have been deposited to Noncentrosymmetric Materials Bank (http://ncsmb.knrrc.or.kr).

## Powder X-ray diffraction (PXRD)

The PXRD data were collected on a Bruker D8-Advance diffractometer using Cu Ka radiation at room temperature with 40 kV and 40 mA. The $2\theta$ range was 5–110° with a step size of 0.02°, and a step time of 1 s. The structures of the reported materials were refined using the Rietveld method with the GSAS program.[9] The refinements of the products were carried out in the NCS space group, $P\bar{6}m2$ (No. 187) with a starting model of the reported single-crystal data of $KCaCO_3F$.[5a] The experimental, calculated, and difference diffraction plots for $KCdCO_3F$ and $RbCdCO_3F$ are shown in Fig. 1. The crystallographic data and refinement results of $ACdCO_3F$ (A = K and Rb) are summarized in Table 1. Atomic coordinates and isotropic displacement parameters of the reported materials can be found in the ESI.†

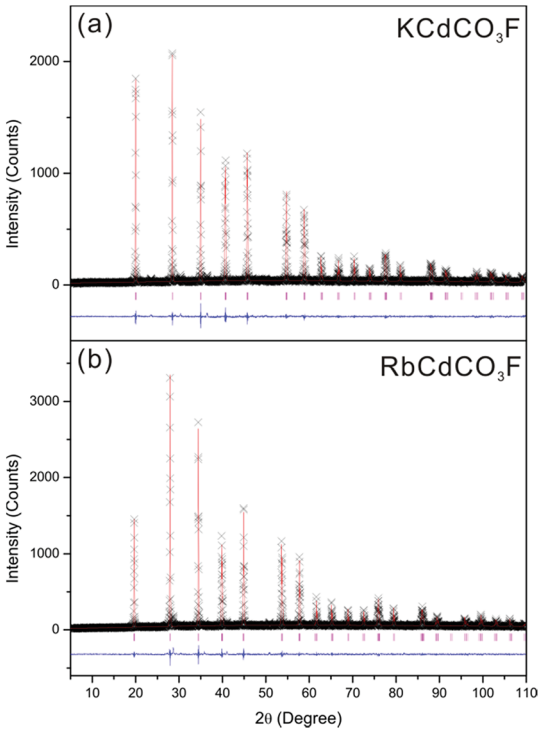


Fig. 1 Experimental, calculated, and difference X-ray diffraction plots for (a) $KCdCO_3F$ and (b) $RbCd(CO_3)_3F$. The calculated pattern (red solid line) is compared with the observed data (×). The locations of the reflections are indicated by the magenta vertical bars. The difference between the observed and calculated profiles is shown at the bottom (blue solid line).

Table 1 Summary of crystallographic data and refinement results of $KCdCO_3F$ and $RbCdCO_3F$

| Formula | $KCdCO_3F$ | $RbCdCO_3F$ |
|---|---|---|
| fw | 230.51 | 276.88 |
| Space group | $P\bar{6}m2$ | $P\bar{6}m2$ |
| $A = b$ Å$^{-1}$ | 5.1287(2) | 5.2101(2) |
| $c$/Å | 4.4277(2) | 4.5293(2) |
| $V$/Å$^3$ | 100.86(11) | 106.48(11) |
| $Z$ | 1 | 1 |
| $R_p$ [a] | 0.1177 | 0.1012 |
| $R_{wp}$ [b] | 0.1633 | 0.1140 |

[a] $R_p = \Sigma|I_o - I_c|/\Sigma I_o$. [b] $R_{wp} = [\Sigma w|I_o - I_c|^2/\Sigma w I_o^2]^{1/2}$.

## Thermal analysis

The thermogravimetric analyses were performed with a Scinco TGA-N1000 thermal analyzer. Reference ($Al_2O_3$) and polycrystalline samples (5–15 mg) were enclosed in $Al_2O_3$ crucibles and heated from room temperature to 800 °C at a rate of 10 °C $min^{-1}$ under a constant flow of argon gas. The TG residues were visually inspected and then analyzed by powder X-ray diffraction after the experiments.

## Infrared (IR) spectroscopy

Infrared spectra of the samples were recorded on a Thermo Scientific Nicolet 6700 FT-IR spectrometer in the 400–4000 $cm^{-1}$ ranges, with the samples embedded in KBr matrices.

### UV-vis diffuse reflectance spectroscopy

UV-vis diffuse reflectance spectra were obtained on a Varian Cary 500 scan UV-vis-NIR spectrophotometer over the spectral range 200–2500 nm at room temperature. The reflectance spectra were transformed into absorbance using the Kubelka–Munk function.[10]

### Second-harmonic generation (SHG) measurements

Powder SHG measurements were carried out using the experimental method adapted from that reported by Kurtz and Perry with 1064 nm radiation.[11] Since SHG efficiencies were known to be strongly dependent on particle size, polycrystalline samples were ground and sieved into the following particle size ranges: 20–45, 45–63, 63–75, 75–90, 90–125, 125–150, 150–200, 250 mm. In order to make relevant comparisons with known SHG materials, crystalline KDP and $KCaCO_3F$ were also ground and sieved into the same particle size ranges. All of the sieved samples with different particle sizes were packed into distinct capillary tubes. The reflected green SHG light with 532 nm was collected and detected using a photomultiplier tube (Hamamatsu). To detect only the SHG light, a 532 nm narrow band-pass interference filter was attached to the front of the tube. The generated SHG signal was monitored using a digital oscilloscope (Tektronix TDS1032). This procedure was then repeated using the standard nonlinear optical materials, *i.e.*, KDP and $KCaCO_3F$, and the ratio of the second-harmonic intensity outputs was calculated. No index-matching fluid was used in any of the experiments. A detailed description of the methodology and the equipment used has been previously published.[12]

### Computational details

Density functional theory (DFT) calculations for $KCdCO_3F$ and $KCaCO_3F$ were conducted by using the Stuttgart tight-binding linear muffin-tin orbital program (TB-LMTO47)[13] with the atomic sphere approximation (ASA). Local density approximation (LDA)[14] was employed to treat exchange and correlation, and a scalar relativistic approximation was used to take into account relativistic effects except spin–orbit coupling. In the ASA method, the space is filled with Wigner–Seitz (WS) atomic spheres,[13] where the symmetry of the potential is considered spherical inside each WS sphere, and a combined correction is used to take into account the overlapping part.[14] The radii of each WS sphere were determined by an automatic procedure[14] and obtained by requiring the overlapping potential be the best possible approximation to the full potential. The overlap should not be too large since the error in kinetic energy introduced by the combined correction is proportional to the fourth power of the relative sphere overlap. Empty spheres should be exploited during the calculations. The used WS radii are as follows: K = 2.387 Å, Cd = 1.640 Å, C = 0.792 Å, O = 0.773 Å, and F = 1.083 Å for $KCdCO_3F$; and K = 2.375 Å, Ca = 1.660 Å, C = 0.850 Å, O = 0.757 Å, and F = 1.070 Å for $KCaCO_3F$. The used basis sets included 4s, 4p, 3d and 4f orbitals for K; 4s, 4p, 3d and 4f orbitals for Ca; 5s, 5p, 4d and 4f orbitals for Cd; 2s, 2p and 3d orbitals for C; 3s, 2p and 3d orbitals for O; and 3s, 2p, and 3d orbitals for F. The K 4p, 3d and 4f, Ca 4p, Cd 4f, C 3d, O 3s and 3d, and F 3s and 3d orbitals were treated by the Löwdin downfolding technique.[15] The *k*-space integrations were conducted by the tetrahedron method,[16] and the self-consistent charge densities for two calculations were obtained using 217 irreducible *k*-points in the Brillouin zone.

## Results and discussion

### Crystal structure description

$KCdCO_3F$ and $RbCdCO_3F$ exhibit similar structures to that of $KCaCO_3F$[5a] and crystallize in the noncentrosymmetric hexagonal space group, $P\bar{6}m2$ (No. 187). As seen in Fig. 2, $ACdCO_3F$ (A = K and Rb) reveal three-dimensional crystal structures consisting of corner-shared $Cd(CO_3)_3F_2$ polyhedra. The $Cd^{2+}$ cations are connected to carbonate groups in the *ab*-plane and are bridged through fluorides along the *c*-direction. The $K^+$ or $Rb^+$ cations are located in the cavities formed by the $Cd(CO_3)_3F_2$ groups. In connectivity terms, the materials may be described as $[Cd(CO_3)_{3/3}F_{2/2}]^-$ anions, with the charge balance maintained by $K^+$ or $Rb^+$ cation. The C atom is coordinated to three O atoms to form a planar $CO_3$ triangle with C–O bond lengths of 1.252(2) Å and 1.255(1) Å for $KCdCO_3F$ and $RbCdCO_3F$, respectively. The cadmium atom is surrounded by six oxygen atoms and two fluorine atoms, forming a highly symmetrical $CdO_6F_2$ hexagonal bipyramid. The $CdO_6F_2$ hexagonal bipyramid shares its six equatorial oxygen atoms with three $CO_3$ groups to form a flat $CdCO_3$ layer and connects adjacent layers with its apical F atoms along the *c*-direction. Within a single $CdCO_3$ layer (Fig. 2(b)), the cooperative connection of hexagonal $CdO_6$ and triangular $CO_3$ makes all $CO_3$ groups aligned parallel in the *ab*-plane and oriented in the same direction. As we will describe more in detail later, the intermolecular interaction between the $d^{10}$ cation, $Cd^{2+}$, and the well aligned π-conjugated group, $CO_3^{2-}$, are responsible for the large macroscopic SHG effect.

The bond valence sums for $ACdCO_3F$ (A = K and Rb) are calculated using the formula,

$$V_i = \sum_j S_{ij} = \sum_j \exp\{(r_0 - r_{ij})/B\}$$

where $S_{ij}$ is the bond valence associated with the bond lengths $r_{ij}$ and $r_0$, and $B$ is an empirically determined parameter (usually 0.37).[17] The calculated bond valence sums for $K^+$, $Rb^+$, $Cd^{2+}$, and $C^{4+}$ are 1.22, 1.39, 1.62–1.72, and 4.32–4.37, respectively.

### Thermal properties

The thermogravimetric analyses (TGA) curves for both samples, $KCdCO_3F$ and $RbCdCO_3F$, show single step weight losses (see Fig. 3). $KCdCO_3F$ is thermally stable up to 320 °C. After that it continually loses weight up to 400 °C. The observed total weight loss of 19.20% is very close to the calculated value of 19.09%. $RbCdCO_3F$ is also stable up to 350 °C, but then it continually loses weight up to 420 °C. The total weight loss of 15.62% is consistent with the calculated value of 15.89%. The weight

 

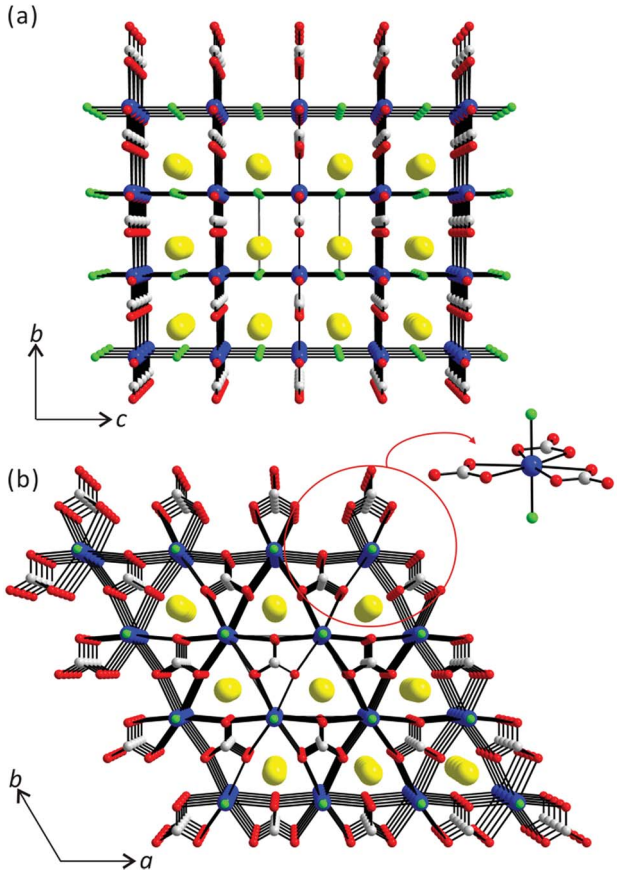


Fig. 2 Ball-and-stick representations of $KCdCO_3F$ (a) viewed along the [100] direction and (b) the $CdCO_3$ layer in the *ab*-plane (blue, Cd; yellow, K; red, O; green, F; gray, C). Note the $Cd^{2+}$ cations exhibit the $Cd(CO_3)_3F_2$ hexagonal bipyramidal coordination environment.

losses correspond to the thermal decomposition of the compounds; in which 1 molecule of $CO_2$ is released from each of the decomposition (see the following reaction). Thermally decomposed residuals were identified as CdO based on the powder X-ray diffraction patterns (see the ESI†).

$$ACdCO_3F\ (A = K \text{ and } Rb) \rightarrow AF + CdO + CO_2\ (g)$$

## Infrared (IR) spectroscopy

The IR spectra of $ACdCO_3F$ (A = K and Rb) revealed C–O vibrations around 1500–650 $cm^{-1}$. The strong broad bands observed at 1432 $cm^{-1}$ for $KCdCO_3F$ and at 1442 $cm^{-1}$ for $RbCdCO_3F$ can be assigned to the C–O stretching vibrations. The out-of-plane vibrations, $\delta$ (OCO), are also observed at 853 $cm^{-1}$ for $KCdCO_3F$ and 843 $cm^{-1}$ for $RbCdCO_3F$ as medium bands. The medium weak bands occurring at about 730–680 $cm^{-1}$ can be assigned to the bending vibrations, $\delta$ (OCO). A strong band observed in the range of 730–680 $cm^{-1}$ may be attributed to the overlap of the bending vibration, $\delta$ (OCO), and the stretching vibration, $\nu$ (Cd–O). The infrared spectra for the reported materials are presented in the ESI.†

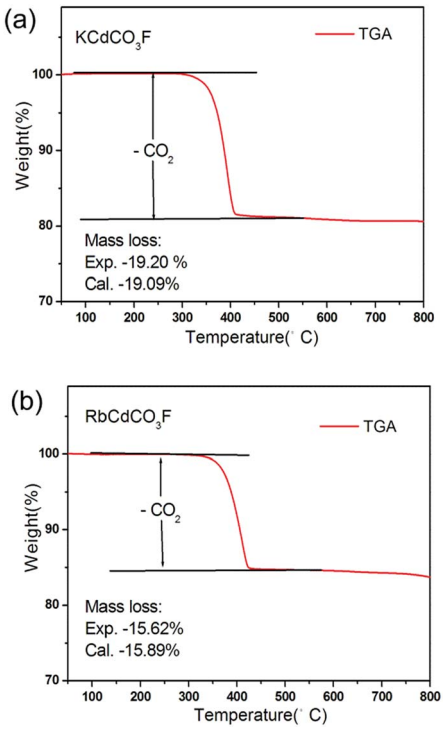


Fig. 3 TGA diagrams of (a) $KCdCO_3F$ and (b) $RbCdCO_3F$.

## UV-vis diffuse reflectance spectroscopy

The UV-vis diffuse reflectance spectra were collected for $ACdCO_3F$ (A = K and Rb) (see Fig. 4). Absorption (*K*/*S*) data were calculated from the following Kubelka–Munk function:

$$F(R) = \frac{(1-R)^2}{2R} = \frac{K}{S}$$

where *R* is the reflectance, *K* is the absorption, and *S* is the scattering.[10] In the (*K*/*S*) *versus E* plots, extrapolating the linear part of the rising curve to zero provides the onset of absorption. The UV absorption spectra exhibit no absorption from 0.25 to 2.5 μm, suggesting that the materials have wide transparent regions ranging from far UV to mid-IR. The optical diffuse reflectance spectra indicate optical band gaps of 5.11 eV for $KCdCO_3F$ and 5.05 eV for $RbCdCO_3F$.

## Nonlinear optical (NLO) properties

The curves of SHG signal as a function of particle size from the measurements made on ground polycrystalline $ACdCO_3F$ (A = K and Rb) are shown in Fig. 5. The results are consistent with phase-matching behaviors according to the rule proposed by Kurtz and Perry (Fig. 5(b)).[11] KDP and $KCaCO_3F$ were used as the reference. $KCdCO_3F$ exhibited very large SHG responses, *ca.* 9 times that of KDP (0.39 pm $V^{-1}$, almost 3 times that of $KCaCO_3F$).[18] Also, the SHG efficiency of $RbCdCO_3F$ turned out to be *ca.* 7.2 times that of KDP (about 2.4 times that of $KCaCO_3F$) (see Fig. 5(a)). It should be noted that the SHG efficiency of $KCdCO_3F$ is the largest reported to date among cadmium compounds containing the planar π-conjugated groups.

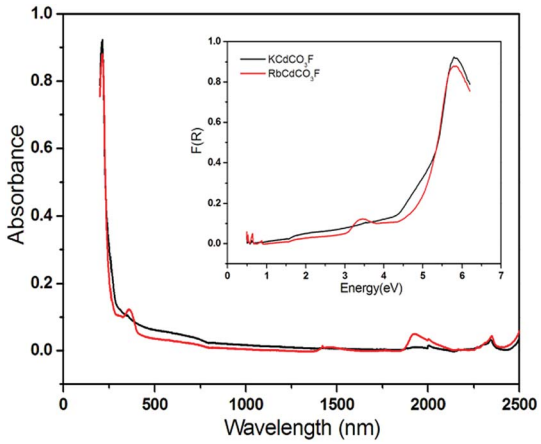


Fig. 4 UV-vis absorption spectra and optical diffuse reflectance spectra of $KCdCO_3F$ and $RbCdCO_3F$.

## Electronic structure calculations

A series of theoretical calculations has been conducted for the title compound $KCdCO_3F$ by using TB-LMTO-ASA method[13] to understand the influence of interatomic interactions between $Cd^{2+}$ cations and the $[CO_3]^{2-}$ units on the $[Cd(CO_3)]_\infty$ layers for the remarkably enhanced SHG response of $KCdCO_3F$. Total and partial density of states (DOS) curves[19] were thoroughly analyzed to understand atomic orbital distributions over the whole energy range, and crystal orbital Hamilton population (COHP) curves[19] were examined as well to study chemical bonding in the structure. Electron localization functions (ELF)[20] visualized the paired electron densities of the interatomic interactions of our interests. $KCaCO_3F$ was also theoretically interrogated for the comparison with the title compound. All details about crystal structures of two compounds were extracted, respectively, from the refinement result of powder X-ray diffraction data of $KCdCO_3F$ and the result of single crystal X-ray diffraction data of $KCaCO_3F$.

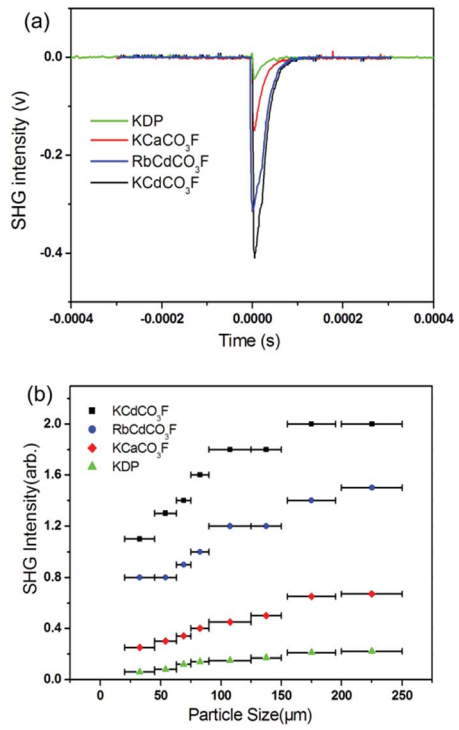


Fig. 5 (a) Oscilloscope traces of the SHG signals for the powders (200–250 μm) of $ACdCO_3F$ (A = K and Rb), KDP, and $KCaCO_3F$. (b) Phase-matching curves for $ACdCO_3F$ (A = K and Rb), KDP, and $KCaCO_3F$ using 1064 nm radiation.

We were particularly interested in the crystallographic *ab*-plane with $y = 0.5$, the (002) plane, where both $Cd^{2+}$ cations and the $[CO_3]^{2-}$ units showed the coplanar alignment and were oriented toward the same direction. In particular, the $[CO_3]^{2-}$ unit had the triangular-shaped local geometry with the $D_{3h}$ symmetry, in which one C atom was located at the center and three O atoms occupied vertices of the triangle. The textbook patterns of DOS curves of the $D_{3h}$ symmetry for the $[CO_3]^{2-}$ units are clearly observed in Fig. 6. The overall total DOS (TDOS) curves display a complex orbital mixing among all three elements. The valence band region below the Fermi level ($E_F$) can be divided into three sections in terms of atomic orbital contributions (see Fig. 6(a)): (1) the section between −9.8 and −6.5 eV includes major contributions from the s, $p_x$, and $p_y$ states of both C and O forming the σ-bond *via* the $sp^2$-hybridization, (2) the section between −5.0 and −1.5 eV displays contributions mostly originated from the $p_z$ state of the central C and the $p_z$ group orbitals of three surrounding O, which eventually form the π-bonding and π*-antibonding in the $[CO_3]^{2-}$ unit (see Fig. 6(b) and (c)), and (3) the region between −1.0 and $E_F$ represents dominant contributions from the nonbonding group orbitals of three O atoms.

As partial DOS (PDOS) curves of Cd (Fig. 6(d)) are projected on PDOS of the just discussed $[CO_3]^{2-}$ unit (Fig. 6(b) and (c)), we can surely realize that the localized d states of Cd appear in the particular region, where the s and p states of both C and O display the major contributions resulting in the σ-bond. On the other hand, the location of the s and p states of Cd overlaps with that of the $p_z$ states of both C and O contributing to the π-bond in the $[CO_3]^{2-}$ unit. It is noteworthy to mention that due to the electronegativity difference between C and O as well as the energy difference of atomic orbitals of C and O, the π-bond contains the larger contribution from O than C. Therefore, this observation implies that a certain degrees of interatomic interactions should exist between $Cd^{2+}$ and the π-conjugated orbitals of the $[CO_3]^{2-}$ unit, and the COHP curves shown in the ESI† well support our interpretation.

This type of particular interatomic interaction on the $[Cd(CO_3)]_\infty$ layers can be visualized by the electron localization function (ELF) diagrams. The ELF has been known to clearly illustrate the paired-electron densities observed in bonding pairs and lone pairs.[20] As mentioned earlier, the sliced (002) plane was selected for our ELF diagram since both $Cd^{2+}$ and the $[CO_3]^{2-}$ unit were located. For the comparison, the ELF plot of the sliced (002) plane for $KCaCO_3F$ was also displayed in Fig. 7. Firstly, the σ-type interactions within the $[CO_3]^{2-}$ unit for both compounds display the nearly identical ELF plot, where large attractors are localized around the $[CO_3]^{2-}$ unit and $Cd^{2+}$,

 

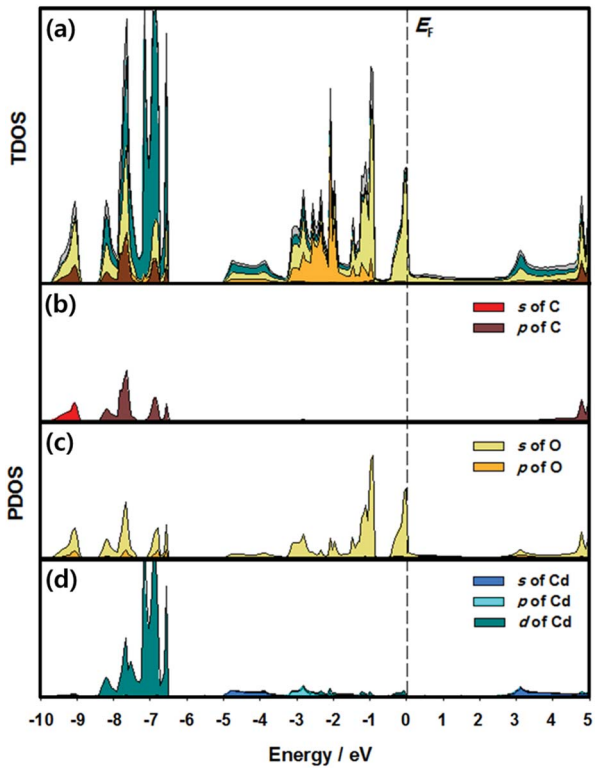


Fig. 6 TDOS curves of $KCdCO_3F$. (a) Total DOS (black-bold line), K PDOS (gray region), Cd PDOS (green region), C PDOS (dark-red region), O PDOS (yellow region), and F PDOS (orange region). $E_F$ is indicated as the vertical dashed line and the energy reference (0 eV). PDOS curves of the selected orbitals for C (b), O (c), and Cd (d), respectively.

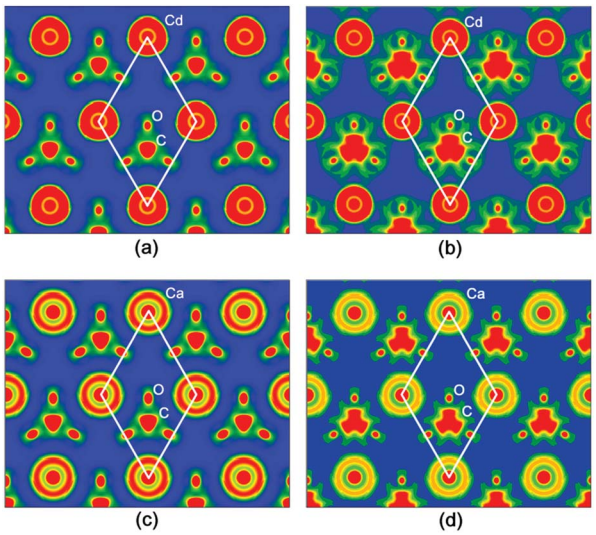


Fig. 7 The electron localization function (ELF) diagrams representing the σ- and the π-bond of $KCdCO_3F$ ((a) and (b)), and $KCaCO_3F$ ((c) and (d)), respectively. The diagrams display sliced-planes of ELF along the (002) direction as contour maps. The color scheme ranges from blue to red (0–0.9), and values higher than 0.5 represent the area exceeding free-electron ELF value.

separately (see Fig. 7(a) and (c)). On the other hand, the π-type interactions inside the $[CO_3]^{2-}$ unit indicate distinctive electron densities for two compounds: the π-conjugated groups of the $[CO_3]^{2-}$ unit in $KCdCO_3F$ spread further out toward $Cd^{2+}$ illustrating certain degrees of interactions between $Cd^{2+}$ and the $[CO_3]^{2-}$ unit (see Fig. 7(b)), whereas those in $KCaCO_3F$ are still confined around the $[CO_3]^{2-}$ unit (see Fig. 7(d)). Therefore, the enhanced SHG response of $KCdCO_3F$ should be attributed to the strengthened interatomic interactions between the s and p states of $Cd^{2+}$ and the π-conjugated groups of the $[CO_3]^{2-}$ unit.

## Structure-NLO properties relationships

$KCdCO_3F$ and $RbCdCO_3F$ crystallize in the NCS nonpolar space group. With the polar materials containing SOJT distortive cations, it has been known that the SHG efficiencies are strongly influenced by the direction and the magnitude of the net moment of polar structural units. However, with the nonpolar materials, the NLO responses of the NCS crystals to an external optical electric field are closely related to the induced dipole oscillations in the lattice. In other words, the compliance of the dipole moment, rather than the intrinsic dipole moment itself, determines the SHG efficiency. Since the compliance of the dipole moment results from the flexibility of the electronic motion in a chemical bond subjected to the perturbation of the external optical electric field, the more "flexible" the chemical bonds in the microscopic groups are, the larger SHG effect in a crystal will be, provided the resulting second-order susceptibility can be additively superposed. On the basis of the anionic group theory, the contribution to the main SHG coefficients of $ACdCO_3F$ (A = K and Rb) from the anionic group $[CO_3]^{2-}$ is dominant. In the structure of $ACdCO_3F$, as we explained in the electronic structure calculations section, the cooperative connection of hexagonal $CdO_6$ and triangular $CO_3$ makes all $CO_3$ groups aligned parallel in the *ab*-plane and oriented in the same direction, giving a 100% optimum to maximize contribution to a large macroscopic SHG effect. In comparison with its isostructural compound $KCaCO_3F$, the sharp SHG increase for $ACdCO_3F$ may have come from polar displacement of a $d^{10}$ cation, $Cd^{2+}$, center as expected. By theoretical calculations, we confirm that the large SHG efficiencies of $ACdCO_3F$ (A = K and Rb) originate from the enhancement *via* interatomic interactions between the s and p states of $Cd^{2+}$ and the π-conjugated groups of the $[CO_3]^{2-}$ unit within the $[Cd(CO_3)]_\infty$ layers. However, no interatomic interaction between $Ca^{2+}$ and the π-conjugated groups of the $[CO_3]^{2-}$ unit in $KCaCO_3F$ is observed.

$KCdCO_3F$ reveals a bit larger SHG efficiency compared to that of $RbCdCO_3F$. The difference may be attributed to the larger polarizability of $Rb^+$ cations that are hampering effective interactions between $Cd^{2+}$ and asymmetric π-systems. $ACdCO_3F$ (A = K and Rb), however, reveal weaker SHG efficiencies compared to that of $CsPbCO_3F$,[5c] although they do exhibit similar crystal structures. More narrow energy gap of $CsPbCO_3F$ (4.15 eV) compared to that of $KCdCO_3F$ (5.11 eV) or $RbCdCO_3F$ (5.05 eV) may results in a stronger interaction between the valence and conduction bands, which can provide extra flexibility of the electronic motion in the delocalized bonds.

## Conclusions

Two phase-matchable NCS compounds, $KCdCO_3F$ and $RbCdCO_3F$ with large powder SHG coefficients and wide transparent regions ranging from far UV to mid IR have been synthesized and characterized. Theoretical analyses reveal that the π-interaction between $Cd^{2+}$ and $[CO_3]^{2-}$ groups within the $[Cd(CO_3)]$ layers are responsible for the remarkable SHG responses. Thus, the reported materials are expected to be promising UV nonlinear optical materials. The growths of large single crystals are ongoing for further physical property measurements.

## Acknowledgements

This work was supported by the National Research Foundation of Korea (NRF) grant funded by the Korea government (No. 2014M3A9B8023478 and 2014H1C1A1066874). G.Z. thanks the National Natural Science Foundation of China (No. 21401178).

## Notes and references

1 (*a*) P. S. Halasyamani and K. R. Poeppelmeier, *Chem. Mater.*, 1998, **10**, 2753; (*b*) H. S. Ra, K. M. Ok and P. S. Halasyamani, *J. Am. Chem. Soc.*, 2003, **125**, 7764; (*c*) R. E. Sykora, K. M. Ok, P. S. Halasyamani and T. E. Albrecht-Schmitt, *J. Am. Chem. Soc.*, 2002, **124**, 1951; (*d*) H. Ye, D. Fu, Y. Zhang, W. Zhang, R. G. Xiong and S. D. Huang, *J. Am. Chem. Soc.*, 2009, **131**, 42; (*e*) S. C. Wang, N. Ye, W. Li and D. Zhao, *J. Am. Chem. Soc.*, 2010, **132**, 8779; (*f*) S. C. Wang and N. Ye, *J. Am. Chem. Soc.*, 2011, **133**, 11458; (*g*) Y. Z. Huang, L. M. Wu, X. T. Wu, L. H. Li, L. Chen and Y. F. Zhang, *J. Am. Chem. Soc.*, 2010, **132**, 12788; (*h*) F. Kong, S. P. Huang, Z. M. Sun, J.-G. Mao and W. D. Cheng, *J. Am. Chem. Soc.*, 2006, **128**, 7750; (*i*) H. Y. Chang, S. H. Kim, P. S. Halasyamani and K. M. Ok, *J. Am. Chem. Soc.*, 2009, **131**, 2426; (*j*) C. F. Sun, C. L. Hu, X. Xu, J. B. Ling, T. Hu, F. Kong, X. F. Long and J.-G. Mao, *J. Am. Chem. Soc.*, 2009, **131**, 9486; (*k*) E. O. Chi, K. M. Ok, Y. Porter and P. S. Halasyamani, *Chem. Mater.*, 2006, **18**, 2070; (*l*) S. L. Pan, J. P. Smit, B. Watkins, M. R. Marvel, C. L. Stern and K. R. Poeppelmeier, *J. Am. Chem. Soc.*, 2006, **128**, 11631; (*m*) S.-W. Bae, C.-Y. Kim, D. W. Lee and K. M. Ok, *Inorg. Chem.*, 2014, **53**, 11328; (*n*) G. Zou, Z. Ma, K. Wu and N. Ye, *J. Mater. Chem.*, 2012, **22**, 19911; (*o*) L. Huang, G. Zou, H. Cai, S. Wang, C. Lin and N. Ye, *J. Mater. Chem. C*, 2015, **3**, 5268.

2 (*a*) P. Becker, *Adv. Mater.*, 1998, **10**, 979; (*b*) C. T. Chen, B. C. Wu, A. D. Jiang and G. M. You, *Sci. Sin., Ser. B*, 1985, **28**, 235; (*c*) C. T. Chen, Y. C. Wu, A. D. Jiang, B. C. Wu, G. M. You, R. K. Li and S. J. Lin, *J. Opt. Soc. Am. B*, 1989, **6**, 616; (*d*) L. Mei, Y. Wang, C. Chen and B. Wu, *J. Appl. Phys.*, 1993, **74**, 7014; (*e*) C. T. Chen, Y. B. Wang, B. C. Wu, K. C. Wu, W. L. Zeng and L. H. Yu, *Nature*, 1995, **373**, 322; (*f*) Y. C. Wu, T. Sasaki, S. Nakai, A. Yokotani, H. G. Tang and C. T. Chen, *Appl. Phys. Lett.*, 1993, **62**, 2614; (*g*) Y. Mori, I. Kuroda, S. Nakajima, T. Sasaki and S. Nakai, *Appl. Phys. Lett.*, 1995, **67**, 1818; (*h*) J. M. Tu and D. A. Keszler, *Mater. Res. Bull.*, 1995, **30**, 209; (*i*) Z. G. Hu, T. Higashiyama, M. Yoshimura, Y. K. Yap, Y. Mori and T. Sasaki, *Jpn. J. Appl. Phys.*, 1998, **37**, 1093; (*j*) R. Komatsu, *Appl. Phys. Lett.*, 1997, **70**, 3492; (*k*) H. Wu, S. Pan, K. R. Poeppelmeier, H. Li, D. Jia, Z. Chen, X. Fan, Y. Yang, J. M. Rondinelli and H. Luo, *J. Am. Chem. Soc.*, 2011, **133**, 7786; (*l*) Y. Shi, S. Pan, X. Dong, Y. Wang, M. Zhang, F. Zhang and Z. Zhou, *Inorg. Chem.*, 2012, **51**, 10870; (*m*) X. Xu, C.-L. Hu, F. Kong, J.-H. Zhang, J.-G. Mao and J. Sun, *Inorg. Chem.*, 2013, **52**, 5831; (*n*) X. Fan, L. Zang, M. Zhang, H. Qiu, Z. Wang, J. Yin, H. Jia, S. Pan and C. Wang, *Chem. Mater.*, 2014, **26**, 3169; (*o*) J.-L. Song, C.-L. Hu, X. Xu, F. Kong and J.-G. Mao, *Angew. Chem., Int. Ed.*, 2015, **54**, 3679; (*p*) H. P. Wu, S. L. Pan, K. R. Poeppelmeier, H. Y. Li, D. Z. Jia, Z. H. Chen, X. Y. Fan, Y. Yang, J. M. Rondinelli and H. S. Luo, *J. Am. Chem. Soc.*, 2011, **133**, 7786; (*q*) H. W. Yu, S. L. Pan, H. P. Wu and Z. H. Yang, *J. Mater. Chem.*, 2012, **22**, 2105; (*r*) H. W. Yu, H. P. Wu, S. L. Pan, Z. H. Yang and K. R. Poeppelmeier, *J. Am. Chem. Soc.*, 2014, **136**, 1264.

3 (*a*) C. T. Chen, *Sci. Sin.*, 1979, **22**, 756; (*b*) C. T. Chen and G. Z. Liu, *Annu. Rev. Mater. Sci.*, 1986, **16**, 203; (*c*) C. T. Chen, Y. C. Wu and R. K. Li, *Int. Rev. Phys. Chem.*, 1989, **8**, 65.

4 N. Mercier, M. Leblanc and J. Durand, *Eur. J. Solid State Inorg. Chem.*, 1997, **34**, 241.

5 (*a*) G. Zou, N. Ye, L. Huang and X. S. Lin, *J. Am. Chem. Soc.*, 2011, **133**, 20001; (*b*) M. Luo, G. Zou, N. Ye, C. S. Lin and W. D. Cheng, *Chem. Mater.*, 2013, **25**, 3147; (*c*) G. Zou, L. Huang, N. Ye, C. S. Lin, W. D. Cheng and H. Huang, *J. Am. Chem. Soc.*, 2013, **135**, 18560.

6 (*a*) T. Tran and P. S. Halasyamani, *Inorg. Chem.*, 2013, **52**, 2466; (*b*) T. Tran, P. S. Halasyamani and J. M. Rondinelli, *Inorg. Chem.*, 2014, **53**, 6241; (*c*) T. T. Tran, J. He, J. M. Rondinelli and P. S. Halasyamani, *J. Am. Chem. Soc.*, 2015, **137**, 10504.

7 (*a*) W. L. Zhang, W. D. Cheng, H. Zhang, L. Geng, C. S. Lin and Z. Z. He, *J. Am. Chem. Soc.*, 2010, **132**, 1508; (*b*) Y. Inaguma, M. Yoshida and T. Katsumata, *J. Am. Chem. Soc.*, 2008, **130**, 6704.

8 D. Phanon and I. Gautier-Luneau, *Angew. Chem., Int. Ed.*, 2007, **46**, 8488.

9 A. C. Larson and R. B. von Dreele, *General Structural Analysis System (GSAS)*, Los Alamos National Laboratory, Los Alamos, NM, 1987.

10 (*a*) P. Kubelka and F. Z. Munk, *Tech. Phys.*, 1931, **12**, 593; (*b*) J. Tauc, *Mater. Res. Bull.*, 1970, **5**, 721.

11 S. K. Kurtz and T. T. Perry, *J. Appl. Phys.*, 1968, **39**, 3798.

12 K. M. Ok, E. O. Chi and P. S. Halasyamani, *Chem. Soc. Rev.*, 2006, **35**, 710.

13 (*a*) O. K. Andersen, *Phys. Rev. B: Condens. Matter Mater. Phys.*, 1975, **12**, 3060; (*b*) O. K. Andersen and O. Jepsen, *Phys. Rev. Lett.*, 1984, **53**, 2571; (*c*) O. K. Andersen, *Phys. Rev. B: Condens. Matter Mater. Phys.*, 1984, **34**, 2439; (*d*) O. Jepsen, A. Burkhardt and O. K. Andersen, *The TB-LMTO-ASA Program, version 4.7*, Max-Plank-Institut fur Festkorperforschung, Stuttgart, Germany, 1999; (*e*)

 

O. K. Andersen, O. Jepsen and D. Glötzel, *Highlights of Cendensed Matter Theory*, North Holland, New York, 1985.
14 O. Jepsen and O. K. Andersen, *J. Phys. Chem. B*, 1995, **97**, 35.
15 R. Dronskowski and P. E. Blöchl, *J. Phys. Chem.*, 1993, **97**, 8617.
16 P. E. Blöchl, O. Jepsen and O. K. Andersen, *Phys. Rev. B: Condens. Matter Mater. Phys.*, 1994, **49**, 16223.
17 (*a*) I. D. Brown and D. Altermatt, *Acta Crystallogr., Sect. B*, 1985, **41**, 244; (*b*) N. E. Brese and M. O'Keeffe, *Acta Crystallogr., Sect. B*, 1991, **47**, 192.
18 R. C. Eckardt, H. Masuda, Y. X. Fan and R. L. Byer, *IEEE J. Quantum Electron.*, 1990, **26**, 922.
19 R. Dronskowski and P. Blöchl, *J. Phys. Chem.*, 1993, **97**, 8617.
20 (*a*) M. V. Putz, *Int. J. Quantum Chem.*, 2005, **105**, 1; (*b*) E. Jang, G. Nam, H. Woo, J. Lee, M.-K. Han, S.-J. Kim and T.-S. You, *Eur. J. Inorg. Chem.*, 2015, **17**, 2786; (*c*) H. Woo, G. Nam, E. Jang, J. Kim, Y. Lee, K. Ahn, S. Bobev and T.-S. You, *Inorg. Chem.*, 2014, **53**, 4669.